A Caledonian Granitoid Pluton at Djupkilsodden, Central Nordaustlandet, Svalbard: Age, Magnetic Signature and Tectonic Significance

By David G. Gee[1], Åke Johansson[2], Alexander N. Larionov[3] and Alexander M. Tebenkov[4]

Abstract: A linear, N-S-trending belt of elliptical, positive magnetic anomalies occurs in central Nordaustlandet, northeast Svalbard. They extend from the Caledonian and older complexes in the vicinity of Duvefjorden, southwards beneath the western margin of Austfonna and the offshore areas covered by Carboniferous and younger strata, to the vicinity of Edgeøya. One of the strongest anomalies occurs in inner Duvefjorden where it coincides with a highly magnetic quartz monzonite–granite pluton at Djupkilsodden. U-Pb and Pb-Pb zircon dating of this post-tectonic pluton defines an age of c. 415 Ma, this being based on the Pb-Pb analyses of three specimens (Pb-Pb ages of 414±10 Ma, 411±10 Ma and 408±10 Ma) and a U-Pb discordia with an upper intercept at 417+18/-7 Ma. Neighbouring felsic plutons in central Nordaustlandet, including the Rijpfjorden and Winsnesbreen granites, lack magnetic signatures in their exposed parts, but have a similar Caledonian age. The central Nordaustlandet magnetic anomalies appear to be part of a *circa* 300 km long linear belt of late Silurian or early Devonian post-tectonic plutonism that characterizes the Caledonian basement of eastern Svalbard. Felsic intrusions of similar age further west in Spitsbergen are likewise both highly magnetic (Hornemantoppen batholith) and largely non-magnetic (Newtontoppen batholith / Chydeniusbreen granitoid suite). They all appear to have been intruded at the end of the main period of Caledonian terrane assembly of the northwestern Barents Shelf.

Zusammenfassung: In Zentral-Nordaustlandet, NO-Svalbard befindet sich eine N-S-gerichtete Zone von elliptischen, positiven magnetischen Anomalien. Die Anomalien erstrecken sich von kaledonischen und älteren Komplexen in der Nähe von Duvefjorden, unter dem westlichen Rand von Austfonna und dem von karbonischen und jüngeren Schichten bedeckten Meeresboden nach Süden bis in die Nähe von Edgeøya. Eine der stärksten Anomalien befindet sich im inneren Duvefjorden, wo sie mit einem stark magnetischen Quarzmonzonit-Granit-Pluton bei Djupkilsodden zusammenfällt. U-Pb und Pb-Pb-Zirkondatierungen dieses posttektonischen Plutons ergeben ein Alter von ca. 415 Ma, wobei dieses Alter auf den Pb-Pb-Analysen von drei Proben basiert (Pb-Pb-Alter von 414±10 Ma, 411±10 Ma und 408±10 Ma) sowie einer U-Pb-Diskordia mit einem oberen Schnittpunkt bei 417 +18/-7 Ma. Benachbarte felsische Plutone in Zentral-Nordaustlandet, einschließlich der Rijpfjorden- und Winsnesbreen-granite, weisen in ihren anstehenden Teilen keine magnetischen Signaturen auf, sie haben jedoch ein ähnliches kaledonisches Alter. Die magnetischen Anomalien in Zentral-Nordaustlandet scheinen ein Teil einer ca. 300 km langen Zone von spätsilurischer oder frühdevonischer posttektonischer Intrusionsaktivität zu sein, die charakteristisch für das kaledonische Grundgebirge Ost-Svalbards ist. Felsische Intrusionen ähnlichen Alters weiter westlich auf Spitzbergen sind ebenfalls teils stark magnetisch (Hornemantoppen Batholith), teils unmagnetisch (Newtontoppen-Batholith / Chydeniusbreen-Granitoid-Suite). Sie scheinen allesamt am Ende der Hauptphase der kaledonischen Orogenese des nordwestlichen Barentsschelfs intrudiert zu sein.

1 David G. Gee, Department of Geophysics, Uppsala University, Villavägen 16, S-752 36 Uppsala, SWEDEN, e-mail: <gee@geofys.uu.se>.

2 Åke Johansson and Alexander N. Larionov, Laboratory for Isotope Geology, Swedish Museum of Natural History, Box 50 007, S-104 05 Stockholm, SWEDEN; e-mail: <ake.johansson@nrm.se> and <alex.larionov@nrm.se.>

4 Alexander M. Tebenkov, Polar Marine Geological Expedition, Pobeda Str. 24, 189510 Lomonosov, RUSSIA; e-mail: <tebenkov.polarex@neva.spb.ru>.

1. INTRODUCTION: MAGNETIC ANOMALIES OF THE NW BARENTS SHELF

The importance of geophysical data, particularly magnetic and preferably in combination with gravity data, for geological mapping and interpretation cannot be overestimated. In the case of the high Arctic geology of the Barents Shelf, the bedrock outcropping onshore provides the foundation for understanding the shallow offshore regions, but interpretation of the latter would hardly be possible without magnetic anomaly maps. The latter exist for the entire Barents Shelf at a scale of 1:1 million (AMAROK A.S. 1994). Large scale versions of magnetic maps have been widely used for geological interpretation both onshore and offshore (e.g. SKILBREI 1992, 1993).

The main geological units of the Svalbard area are shown on Fig. 1, and magnetic anomaly data on Fig. 2. Comparison of these maps shows that the main positive magnetic anomalies correlate with rock units in the pre-Devonian basement. Some of these anomalies can be followed beneath the younger strata on Svalbard and out beneath the Barents Shelf. Thus their identification onshore is of fundamental importance for the regional interpretation offshore.

Svalbard's magnetic anomalies are dominated by a central N-S-trending positive linear feature (A on Fig. 2) located along the western margin of Ny Friesland (SKILBREI 1992, 1993). It apparently terminates in the north, offshore, in a circular positive anomaly (B on Fig. 2). To the south, it fades away under the Mesozoic to Tertiary basin in central Spitsbergen. However, it apparently re-appears along strike, off the southeast coast of Spitsbergen (C on Fig. 2, cf. SKILBREI 1992), which gives it a total strike length of at least 500 kilometres. In Ny Friesland, this anomaly is unambiguously related to magnetite-rich late Paleoproterozoic *(circa* 1750 Ma) granitic rocks that occur in the Atomfjella antiformal thrust-stack (WITT-NILSSON et al. 1998). These gneissic granites are present at at least three structural levels, but are most prominent in the Nordbreen Nappe (the Bangenhuk granitoids, cf. JOHANSSON et al. 1995, CARLSSON et al. 1995) in the W-dipping limb of the antiform. The latter is truncated by a major N-S-trending fault in Wijdefjorden (the Billefjorden Fault). These Palaeoproterozoic granites have high magnetic susceptibilities (1200-12500 x 10⁻⁵ SI-units; SKILBREI 1993, TEBENKOV 1996 and unpublished data), far in excess of other rock units of regional significance in the area, including the numerous amphibolites. The high susceptibilities are most
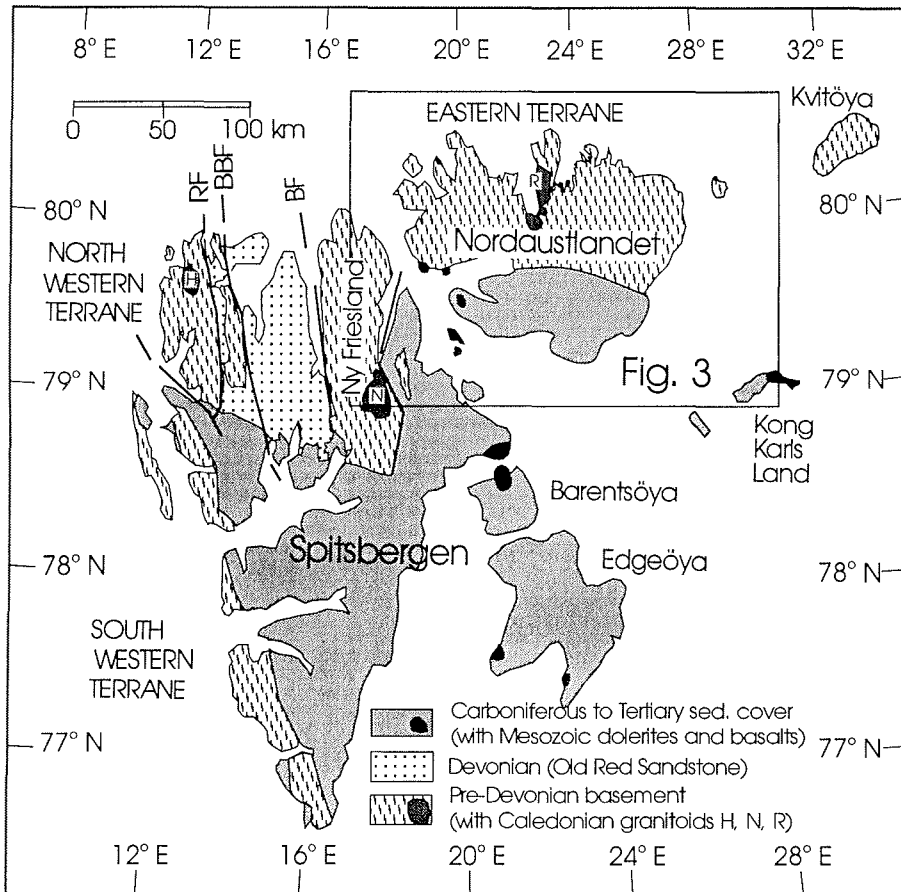
Fig. 1: Main geological units of Svalbard, including the different Caledonian terranes, with terrane boundaries after GEE (1986). Main Caledonian fault zones: RF = Raudfjorden Fault, BBF = Breibogen-Bockfjorden Fault, BF = Billefjorden Fault. Main Caledonian granitoids: H = Hornemantoppen batholith, N = Newtontoppen batholith (Chydeniusbreen suite) , R = Rijpfjorden granite.

Abb. 1: Geologische Haupteinheiten von Svalbard, einschließlich der verschiedenen kaledonischen Terrane, nach GEE (1986). Kaledonische Hauptstörungszonen: RF = Raudfjorden-Störung, BBF = Breibogen-Bockfjorden-Störung, BF = Billefjorden-Störung. Wichtigste kaledonische Granitoide: H = Hornemantoppen Batholith, N = Newtontoppen Batholith (Chydeniusbreen-Suite), R = Rijpfjorden-Granit.
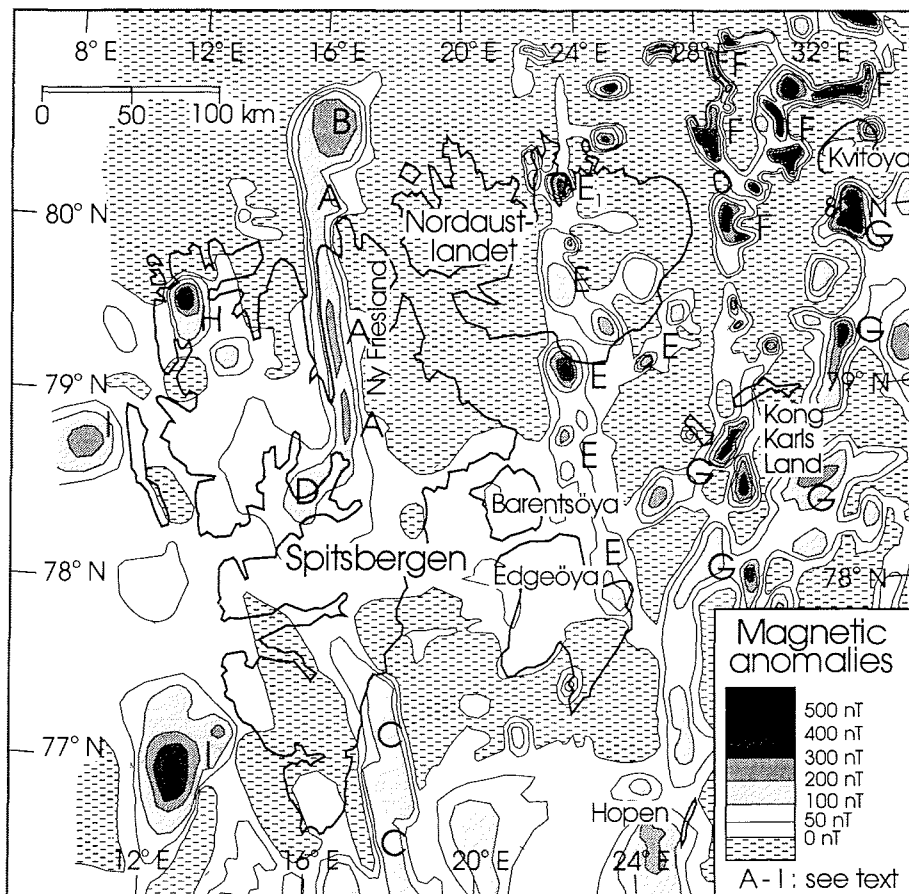

Fig. 2: Magnetic anomalies of Svalbard and the northwestern Barents Shelf, simplified from the 1:1 million aeromagnetic anomaly map of the northwestern Barents Shelf by AMAROK A.S. (1994). A-I = magnetic anomalies discussed in the text.

Abb. 2: Magnetische Anomalien von Svalbard und des nordwestlichen Barentsschelfs, vereinfacht von der aeromagnetischen Anomaliekarte des nordwestlichen Barentsschelfs (1:1 000 000) von AMAROK A.S. (1994). A-I = magnetische Anomalien, die im Text diskutiert werden.

probably caused by magnetite, a mineral also observed to occur frequently as idiomorphic grains in neosome-rich parts of the migmatitic Eskolabreen granitic gneisses within the lowermost structural level (JOHANSSON & GEE, in press).

The Ny Friesland anomaly passes south and merges into a near circular major anomaly (D on Fig. 2) centered on inner Isfjorden. The source of the latter is not known, but based on depth estimates, it is apparently related to the basement beneath the Devonian Old Red Sandstone graben of Andrée Land and the Carboniferous to Tertiary basin in central Spitsbergen (SKILBREI 1992). Further to the northwest, a prominent elliptical anomaly (H on Fig. 2) coincides with the location of the highly magnetic Caledonian Hornemantoppen batholith (HJELLE 1979, SKILBREI 1993, BALASOV et al. 1996, H on Fig. 1). It is tempting to relate other circular or elliptical anomalies in buried or offshore parts of the Svalbard basement, such as B or D, to Caledonian granitoids. However, not all Caledonian granites appear to be magnetic; neither the Chydeniusbreen granitoid suite (including the major Newtontoppen batholith) of southern Ny Friesland (TEBENKOV et al. 1996, N on Fig. 1) nor the Rijpfjorden granite of north-central Nordaustlandet (R on Fig. 1) show up as significant positive magnetic anomalies on Fig. 2.

East of the prominent linear Ny Friesland anomaly (A) is a wide low magnetic area in eastern Ny Friesland and western Nordaustlandet, coinciding with the Neoproterozoic sedimentary rocks of the Lomfjorden and Murchisonfjorden Supergroups and the Grenville-age volcanic and granitic rocks of northwestern Nordaustlandet. By contrast, central Nordaustlandet is characterised by a linear N-trending belt of elliptical anomalies (E on Fig. 2) that appear to extend far to the south towards Edgeøya, beneath the Carboniferous and younger strata of eastern Svalbard. These anomalies are the focus of this article, which concentrates on one of the most prominent positive features, a high of circa 330 nT (E_1 on Fig. 2) centred on inner Duvefjorden (cf. Fig. 3).

Offshore to the east and southeast of Svalbard there are a variety of strong positive anomalies. They are particularly prominent in the area between Nordaustlandet and Kvitøya (F on Fig. 2) and to the north of this island. Further to the south, a NE-trending belt (G on Fig. 2) of elliptical anomalies crosses Kong Karls Land. The extensive development of Upper Jurassic and Lower Cretaceous basalts on these islands (BAILEY & RASMUSSON 1997) suggests that these anomalies are related to Mesozoic rift-related volcanism. High-frequency magnetic anomalies in the Svalbard area are apparently caused by such mafic rocks (J.R. Skilbrei, pers. comm. 1998). The anomalies further to the north (F on Fig. 2) may likewise be of Mesozoic age; however, since no high positive magnetic anomalies are associated with the Mesozoic dolerites exposed on Nordaustlandet and adjacent islands, this suggestion is speculative. Two strong elliptical positive anomalies off the west-coast of Spitsbergen (I on Fig. 2) have tentatively been suggested to be caused by Tertiary intrusions related to break-up and separation of Svalbard from northeast Greenland and the formation of the North Atlantic Ocean (SKILBREI 1992).

2. NORDAUSTLANDET GEOLOGY

Much of Nordaustlandet is covered by extensive ice caps. Carboniferous and younger successions are exposed in the southern part, and Caledonian basement rocks in the northern part, of the island (Fig. 3). Cambrian strata, underlain by Svalbard's classical Vendian tillite-bearing Sveanor Formation (KULLING 1934), outcrop in the west beside Hinlopenstretet (Hinlopenstretet Supergroup). These are, in turn, underlain by an extensive Neoproterozoic carbonate and sandstone-shale succession (Murchisonfjorden Supergroup, Tab. 1). The strata are little metamorphosed and are deformed by upright to W-vergent folds that plunge gently to the south. A major anticlinorium dominates the Vestfonna area and older rocks outcrop along the north coast and further to the east.

In the northwestern part of Nordaustlandet, in rock units inferred to underlie the Murchisonfjorden Supergroup, a conglomerate was recognised on Botniahalvøya (FLOOD et al. 1969) to separate greenschist facies volcanic and sedimentary rocks. OHTA (1982) demonstrated that the volcanic rocks (Kapp Hansteen Group) were younger than the folded metasediments (Brennevinsfjorden Group); however the relationship of the former to the Murchisonfjorden Supergroup strata was not established, the contact being located in Lady Franklinfjorden (Fig. 3) and probably faulted. Granites, intruded into the Brennevinsfjorden Group, were shown to be late Grenvillian (circa 950 Ma) in age (GEE et al. 1995).

WESTERN AREA (GEE ET AL. 1995)	CENTRAL AREA (GEE & TEBENKOV 1996)
Hinlopenstretet Supergroup (Vendian-Cambrian metased.)	
Murchisonfjorden Supergroup (Neoproterozoic metasediments)	
----------------------- *unconformity* -----------------------	
Kapp Hansteen Group (Grenvillian metavolcanites)	Svartrabbane Formation (Grenvillian metavolc.)
----------------------- *unconformity* -----------------------	
Brennevinsfjorden Group (Mesoproterozoic metased.)	Helvetesflya Formation (Mesoproterozoic metased.)
unknown basement	unknown basement

Tab. 1. Main stratigraphic units of Nordaustlandet, based on GEE et al. (1995; western area) and GEE & TEBENKOV (1996; central area) and unpublished isotopic age data (JOHANSSON & LARIONOV, in prep.).

Tab. 1: Stratigraphische Haupteinheiten von Nordaustlandet, nach GEE et al. (1995; westlicher Teil) und GEE & TEBENKOV (1996; zentraler Teil) und unveröffentlichten Isotopendaten (JOHANSSON & LARIONOV, in Vorber.).

Recent investigations in central Nordaustlandet (GEE & TEBEN-KOV 1996) have shown that the Murchisonfjorden Supergroup overlies the older complex with a major unconformity separating them. This complex is composed of both volcanic (Svartrabbane Formation) and sedimentary (Helvetesflya Formation) rocks metamorphosed in greenschist facies. A second major unconformity separates the volcanic from the sedimentary rocks, the former overlying the latter (Tab. 1). The Helvetesflya Formation was folded and intruded syntectonically by granites (GEE, in FLOOD et al. 1969).

Previous work and unpublished geochronological data, summarized by JOHANSSON & LARIONOV (1996), have demonstrated that Nordaustlandet's bedrock geology is dominated by a Grenvillian-age (possibly also older) basement complex, with granites and metavolcanic and metasedimentary rocks, unconformably overlain by a thick Neoproterozoic to early Palaeozoic succession (Tab. 1, Fig. 3). In eastern Ny Friesland, the latter reaches up into the middle Ordovician and the folding is probably Silurian in age.

Many of the granites in Nordaustlandet's basal complex are high-ly deformed, partly syntectonic and demonstrably Grenvillian in age. They are cut by younger "post-tectonic", little deformed felsic plutons that are not seen to intrude the Murchisonfjorden Supergroup and could be of Proterozoic or Palaeozoic age. The largest of these intrusions is the Rijpfjorden granite of north-central Nordaustlandet (Figs. 1, 3; FLOOD et al. 1969), which appears to be non-magnetic (Fig. 2). A smaller intrusion, here referred to as the Djupkilsodden Pluton, coincides with the onshore part of the prominent Duvefjorden magnetic anomaly (E_1 in Fig. 2), and forms the main subject of this paper.

3. THE DJUPKILSODDEN PLUTON

3.1. *Field relations*

Field investigations of the post-tectonic intrusions of Djupkils-odden (Fig. 4) were carried out by two of us (DGG and AMT) in 1995. Time permitted only a brief two-day reconnaissance for sampling and measurement of magnetic susceptibility, and a more thorough investigation is warranted. Nevertheless, it was
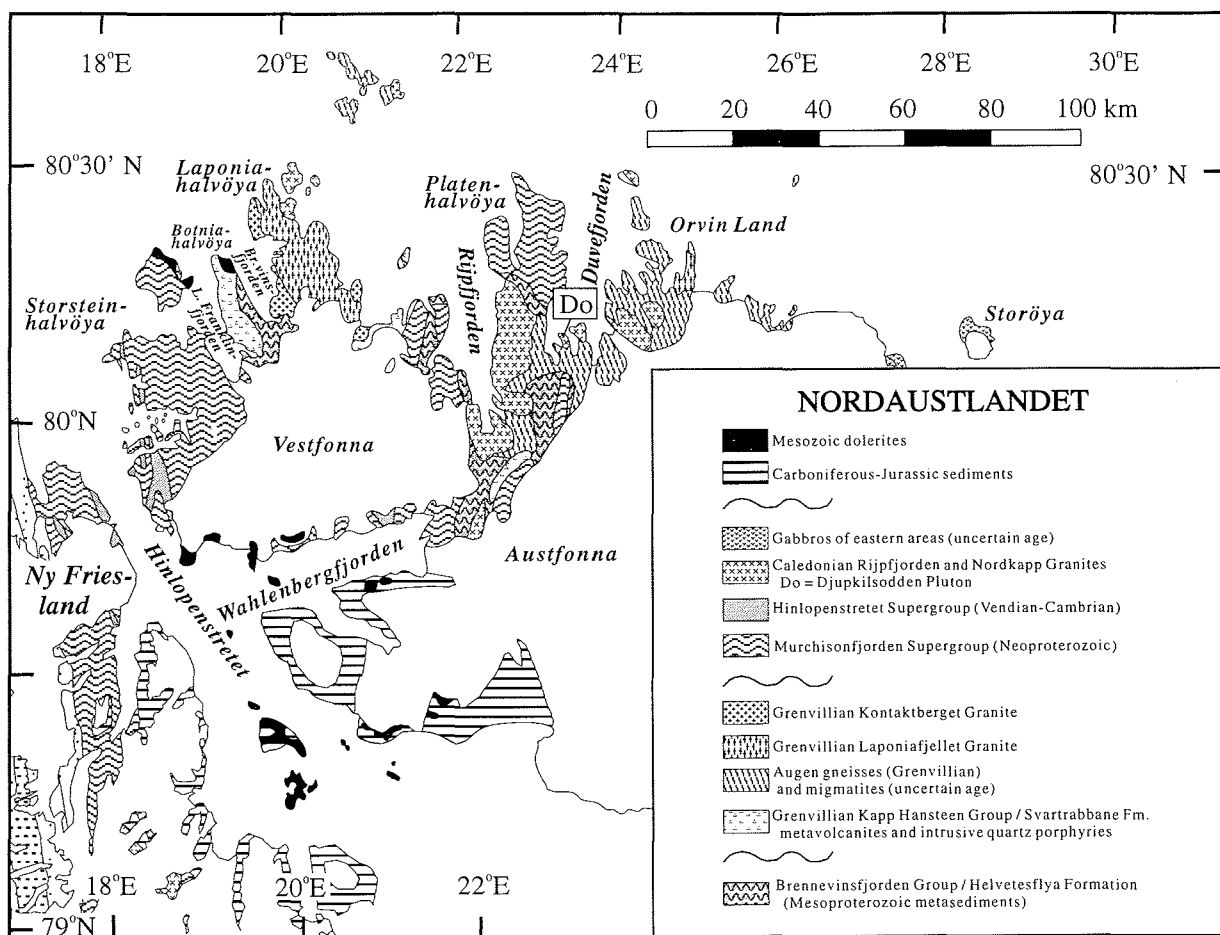

Fig. 3: Geology of Nordaustlandet, based on FLOOD ET AL. (1969), HJELLE & LAURITZEN (1982) and LAURITZEN & OHTA (1984), with local modifications. Do = Djupkilsodden Pluton.

Abb. 3: Geologie von Nordaustlandet, nach FLOOD ET AL. (1969), HJELLE & LAURITZEN (1982) und LAURITZEN & OHTA (1984), mit lokalen Veränderungen. Do = Djupkilsodden-Pluton.
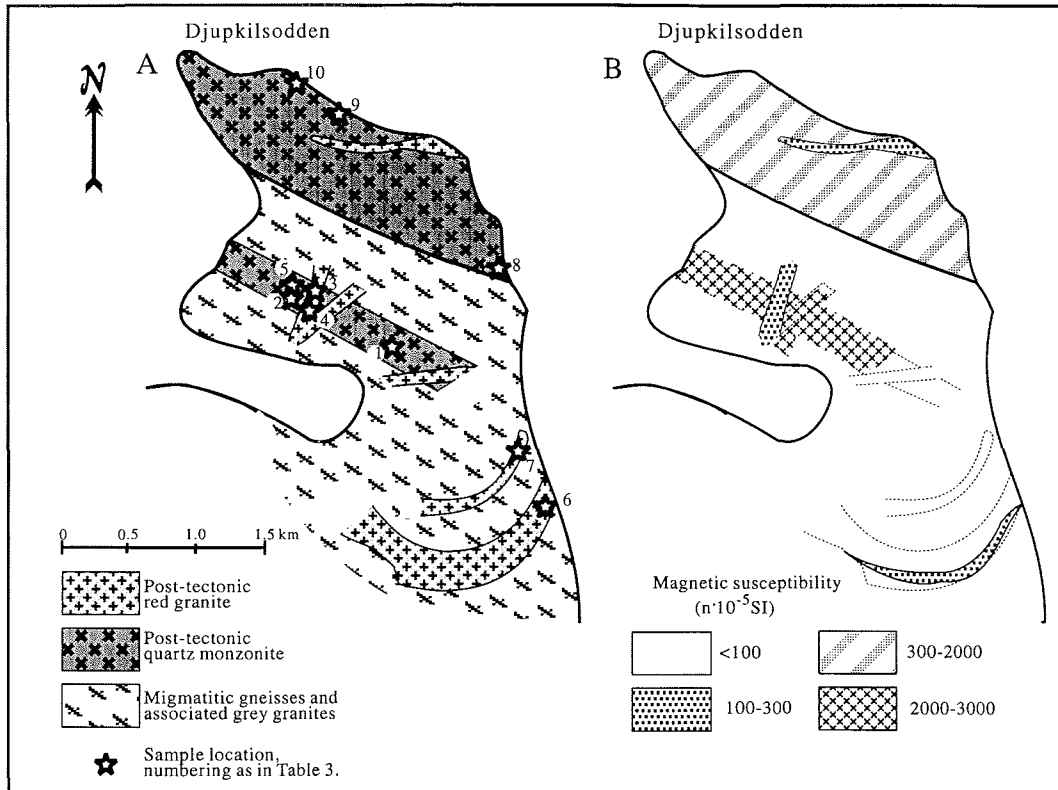
Fig. 4: Detailed geological map (**A**) and magnetic susceptibility map (**B**) of the Djupkilsodden Pluton.

Abb. 4: Detaillierte geologische Karte (**A**) und Karte über die magnetische Suszeptibilität (**B**) des Djupkilsodden-Plutons.

possible to define the approximate distribution of the intrusions, the latter being dominated by quartz monzonites cut by subordinate granites. In marked contrast to the neighbouring Rijpfjorden granites, the Djupkilsodden quartz monzonites proved to be strongly magnetic and even some of the associated granites had high susceptibilities. The main body of the intrusion occurs in the northern part of the Djupkilsodden peninsula (Fig. 4A) and apparently extends eastwards across Djupkilen to Louise Richardfjellet (see FLOOD et al. 1969) and northwards into inner Duvefjorden (Fig. 3).

The Djupkilsodden quartz monzonites are intruded into migmatites and foliated grey gneisses (Fig. 4A) that structurally underlie the metasedimentary and metavolcanic rocks of the Helvetesflya and Svartrabbane Formations (GEE & TEBENKOV 1996), the latter outcropping south of Innvika (Fig. 3). The migmatites generally have a dominating foliation, dipping gently beneath the supracrustal rocks in the vicinity of Innvika, and increasing in angle to near-vertical, with NW-SE strike, near the Djupkilsodden Pluton. The contact between the plutonic rocks and the migmatites and associated grey gneissic granites is generaly knife-sharp and steep, trending WNW across the peninsula. To the south of this contact, there occur sheets of both quartz monzonite and reddish granite. All rock units are intruded by aplites and pegmatites and a few dark biotite lamprophyres.

3.2. Magnetic susceptibility

The measurement of magnetic susceptibility has been made directly in the field by magnetic susceptibility meter (Fiskars Geoinstruments JH-8, calibrated at the Geological Survey of Sweden). The obtained results are shown in Table 2 and on Fig. 4B.

Rock type	Magnetic susceptibility (n x 10^{-5} SI-units)	Number of measurements
Migmatite	10 - 90	60
Red granite (non-magnetic)	1 - 10	50
Red granite (magnetic)	100 - 300	30
Quartz monzonite	200 - 3000	50
Pegmatite	10 - 50	10
Lamprophyre	200 - 1000	10

Tab. 2: Magnetic susceptibility of the Djupkilsodden granitoids and surrounding country rocks, north-central Nordaustlandet, Svalbard.

Tab. 2: Magnetische Suszeptibilität der Djupkilsodden-Granitoide und umgebender Gesteine, nördlicher Teil von Zentral-Nordaustlandet, Svalbard.

The migmatites, pegmatites and most of the red granites are low magnetic (below 100 x 10^{-5} SI-units) while the quartz monzonites, the lamprophyres and part of the red granites are highly magnetic, reaching up to 3000 x 10^{-5} SI-units (Table 2). According to the aeromagnetic map (Fig. 2), a more or less isometric positive anomaly is located in the southern part of Duvefjorden with its centre just north of the Djupkilsodden peninsula. There is no doubt that the main source of this positive aeromagnetic anomaly is related to the quartz monzonite, the magnetic signature of which contrasts strongly with the surrounding rocks. The small volumes of the lampophyre dikes and the magnetic variability of the granites make their overall contribution to the anomaly subordinate. The shape and location of the anomaly indicate that the main outcrop of high-magnetic granitoids continues from Djupkilsodden some distance to the north under the waters of Duvefjorden and probably eastwards to the Louise Richardfjellet peninsula.

3.3 *Petrography and petrochemistry*

The two main types of felsic intrusive rocks at Djupkilsodden, grey quartz monzonites and red granites, were collected for isotope age determination studies and complementary work on petrography and petrochemistry.

The *grey quartz monzonites* are massive medium- to coarse-grained hypidiomorphic rocks. Their modal composition is: quartz 10-20 %, plagioclase (albite) 25-30 %, K-feldspar 15-20 %, biotite (main dark mineral; brown and usually idiomorphic) 20-30 %, opaque minerals, probably mainly magnetite 1-3 %, and titanite 1-3 %. Accessories are represented by apatite, zircon, and rare tourmaline. Secondary chlorite (usually less than 1 %, in a few thin sections up to 3 %) occurs after biotite. Quartz sometimes has sutured boundaries and the feldspar is generally sericitized. The titanite occurs as rims surrounding the ore minerals as well as in independent aggregates and rare idiomorphic grains.

The *red granites* differ from the quartz monzonites in being more leucocratic, with less than 10 % biotite and additional minor muscovite. Monazite, as well as titanite and zircon, were recovered during mineral separation of granite sample G95:039.

Petrochemical analyses of major elements were made by the XRF method at Polar Marine Geological Expedition, Lomonosov, with Fe_2O_3 being analysed separately by wet chemical methods at VNII Oceangeology, St. Petersburg. The results are reported in Tab. 3 and illustrated in Fig. 5, after recalculation to an anhydrous base. On the petrochemical classification diagrams, the red granites plot as granite (Figs. 5B, 5C and 5D), while the grey quartz monzonites are located in the quartz syenite (Fig. 5B) or quartz monzonite (Fig. 5C) field, or on the border between granite and adamellite (Fig. 5D). The granites are peraluminous while the quartz monzonites plot close to the boundary between metaluminous and peraluminous rocks, but mainly on the metaluminous side (Fig. 5E). Both varieties plot as S-type granitoids (Fig. 5F). On the tectonic discrimination diagram of BATCHELOR & BOWDEN (1985; Fig. 5A) the quartz monzonites are located on the boundary between the "post-collision uplift" and "late-orogenic" fields, while the red granites trend from the "late-orogenic" towards the "syn-collision" field.

4. Pb-Pb AND U-Pb ISOTOPE AGES

4.1 *Mineral descriptions*

Zircons, titanite and monazite were separated from the rock samples using standard techniques.

Quartz monzonite samples G95:038 and G95:040
Eu- and subhedral zircons, mainly prismatic, with length/width ratios between 1.5 and 4, occasionally up to 6, are found. The zircons are generally pink or yellowish, some are colourless. They are dominantly turbid and fractured, but ocassionally trans-

No on Fig 4	Sample Number	Rock Type	SiO2	TiO2	Al2O3	Fe2O3	FeO	MnO	MgO	CaO	Na2O	K2O	P2O5	LOI	SUM
1	59-3T95	Q-Monzonite	60,12	1,52	15,79	1,42	4,68	0,08	2,03	2,90	2,61	5,59	0,88	1,42	99.04
2	60-1T95 (G95038)	Q-Monzonite	60,29	1,32	14,66	2,47	3,51	0,10	2,59	3,34	2,66	5,89	0,91	1,29	99.03
3	60-2T95 (G95039)	Granite	72,82	0,17	13,91	1,09	1,18	0,00	0,12	0,56	2,92	6,09	0,06	0,23	99.15
4	60-3T95	Granite	67,90	0,34	15,25	2,10	1,59	0,08	0,21	0,58	3,49	6,62	0,06	0,58	98.80
5	60-4T95	Q-Monzonite	64,16	1,15	14,56	1,93	3,05	0,07	1,22	2,63	2,84	5,83	0,66	1,04	99.14
6	61-1T95	Granite	70,95	0,32	14,04	0,82	2,08	0,02	0,19	0,97	2,95	6,27	0,13	0,43	99.17
7	61-3T95	Granite	67,17	0,68	14,89	1,22	2,74	0,05	0,51	1,64	2,77	6,67	0,29	1,00	99.63
8	61-4T95	Q-Monzonite	64,00	1,18	15,45	1,48	3,96	0,08	1,08	2,83	3,12	5,37	0,56	0,64	99.75
9	61-5T95	Q-Monzonite	61,23	1,34	14,98	1,79	4,14	0,10	2,35	2,94	2,64	5,83	0,87	0,86	99.07
10	61-6T95 (G95040)	Q-Monzonite	60,62	1,29	15,59	2,05	3,66	0,10	2,34	3,42	2,56	5,93	0,89	1,01	99.46

Tab. 3: Bulk chemistry composition of the Djupkilsodden granitoids, north-central Nordaustlandet, Svalbard. Analyses by XRF at Polar Marine Geological Expedition, Lomonosov. Fe_2O_3 analysed by wet chemistry at VNII Oceangeology, St. Petersburg.

Tab. 3: Chemische Zusammensetzung der Djupkilsodden-Granitoide, nördlicher Teil von Zentral-Nordaustlandet, Svalbard.

A Batchelor & Bowden 1985 (fig 10)

1 - Mantle Fractionates
2 - Pre-plate Collision
3 - Post-collision Uplift
4 - Late-orogenic
5 - Anorogenic
6 - Syn-collision
7 - Post-orogenic

$R2 = 6Ca + 2Mg + Al$

$R1 = 4Si - 11(Na + K) - 2(Fe + Ti)$

B Debon & Le Fort 1983 (fig 1)

1 - Granite
2 - Adamellite
3 - Granodiorite
5 - Qz syenite

$Q = Si/3 - (K + Na + 2Ca/3)$

$P = K - (Na + Ca)$

C Middlemost 1985 (fig 3.3.6)

3 - Alkali fsp granite
5 - Qz syenite
6 - Granite
8 - Qz monzonite
11 - Granodiorite

$Na2O + K2O$ (wt %)

$SiO2$ (wt %)

D

Anorthite

A: Tonalite
B: Granodiorite
C: Adamellite
D: Trondhjemite
E: Granite

Albite   Orthoclase

E Maniar & Piccoli 1989 (fig 2)

Metaluminous   Peraluminous

Peralkaline

$Al2O3/(Na2O + K2O)$

$Al2O3/(CaO + Na2O + K2O)$

F

$K2O$ (wt %)

S-type   R   I-type   H   N

$Na2O$ (wt %)

■ Djupkilsodden qz-monzonites   × Newtontoppen granosyenites

● Djupkilsodden granites   + Newtontoppen granites

○ Hornemantoppen granitoids   ⊔ Newtontoppen aplites

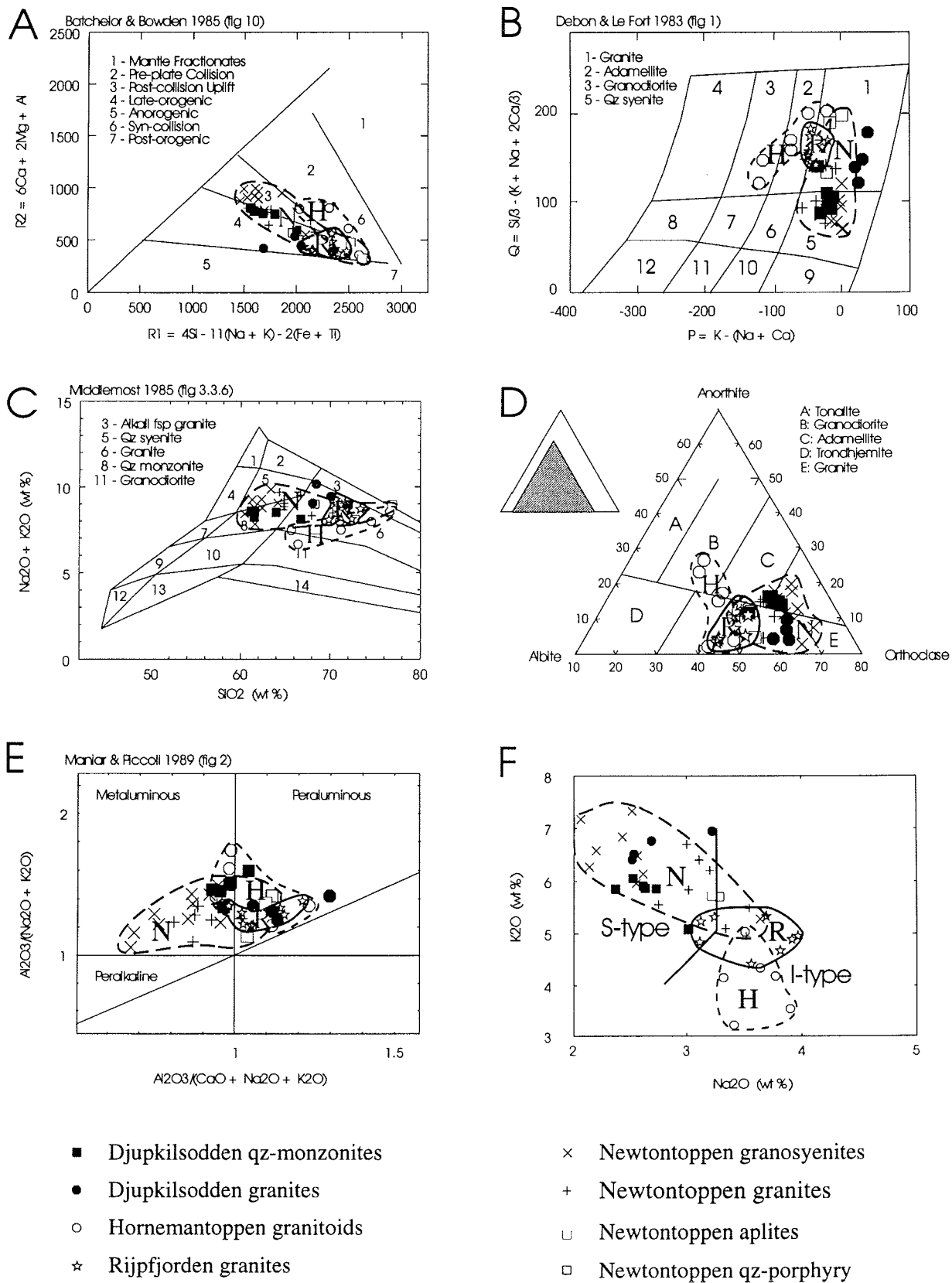☆ Rijpfjorden granites   ◻ Newtontoppen qz-porphyry

Fig. 5: Geochemical classification diagrams of the Djupkilsodden granitoids compared to other Caledonian granitoids of Svalbard. Data on the Hornemantoppen batholith (H) from BALASOV ET AL. (1996), on the Newtontoppen batholith (N) from TEBENKOV ET AL. (1996), and the Rijpfjorden granite (R) from LARIONOV ET AL. (1998).

Abb. 5: Geochemische Klassifizierungsdiagramme der Djupkilsodden-Granitoide, verglichen mit anderen kaledonischen Granitoiden von Svalbard. Daten für den Hornemantoppen-Batholith (H) nach BALASOV ET AL. (1996), für den Newtontoppen-Batholith (N) nach TEBENKOV ET AL. (1996), und für den Rijpfjorden-Granit (R) nach LARIONOV ET AL. (1998).

parent (Fig. 6A-B). Growth zoning and overgrowths at termi-nations have been observed in some grains. Black flake-shaped inclusions (bioitite ?) are quite common, while orange-colou-red inclusions occur rarely.

Granite sample G95:039

Zircons are subhedral or euhedral, with length/width ratios be-tween 2 and 4. Facet surfaces are usually smooth, but sometimes rough, probably due to resorbtion. The zircons are brown, greyish, pink, sometimes colourless, and translucent to turbid, with only a few grains being transparent (Fig. 6C). Possible cores have been observed in some grains, and overgrowths at terminations have been noted. Black flake-shaped and orange-coloured inclusions are quite common. The zircon morphology indicates their mag-matic origin, while the high amount of turbid grains suggests metamictization, due to high U and Th contents.

Titanite from the same sample consists of prismatic, transparent to translucent or even turbid grains with rough surfaces and yellow to orange colour. Monazite consists of yellow, transpa-rent, flat or irregular, small grains with smooth surfaces.

4.2 *Single-zircon Pb evaporation analyses*

Single-zircon $^{207}Pb/^{206}Pb$ analyses have been performed follow-ing the procedure proposed by KOBER (1986). Descriptions of the analytical technique used at the Laboratory for Isotope Geo-logy in Stockholm and the procedures for calculating the ages are found in GEE & HELLMAN (1996), HELLMAN et al. (1997) and LARIONOV et al. (1998). The full analytical results are found in Appendix 1.

Four zircons from quartz monzonite sample G95:038 have been analysed. Results from two to five evaporation steps have been recorded. The total number of blocks measured was 54. The $^{207}Pb/^{206}Pb$ ages fall between 385 and 462 Ma, with most of them within the range 400-420 Ma (Fig. 7A). Exclusion of a few out-liers gives an average age of 414 ±10 Ma.

From quartz monzonite sample G95:040, four zircons have been analysed, with 61 blocks recorded. The corrected $^{207}Pb/^{206}Pb$

ratios correspond to ages between 314 and 434 Ma (Fig. 7B). Inspection of Fig. 7B suggests that there is a stable plateau age, displayed by grains A, B and D, slightly above 400 Ma, while the ages below 400 Ma represent discordant lead expelled from metamict parts of the zircons during the first heating steps. An average age calculated on 36 blocks which fall into the age span 400-420 Ma, is 411 ±10 Ma, while a calculation for the broader interval 380-420 Ma (47 blocks) gives 403 ±20 Ma.

Three zircons from granite sample G95:039 have been analy-sed, but only data from two of these were used for the average age calculation. The third grain, C (Fig. 7C) shows considera-ble scatter in the results, possibly due to complexities in its struc-ture. The total age range is 377-454 Ma, excluding one block from the first heating step with lead from metamict zircon. 15 blocks out of 25 give the average age of 408 ±10 Ma.

The somewhat lower ages obtained for some blocks from the zircons of sample G95:040 compared with sample G95:038 may reflect higher Pb-loss from the former zircons due to a more metamict structure, or problems with the common lead correc-tion due to higher common lead contents. The steps which show ages older than 420 Ma may reflect inherited domains within the zircons, in agreement with the presence of Grenvillian rocks in the area (JOHANSSON & LARIONOV 1996, unpub. data), as well as with the results from the Caledonian Rijpfjorden granite (*op. cit.*).

4.3 *U-Pb multi-grain analysis*

Zircons from four different size fractions from quartz monzo-nite sample G95:038 and three size fractions from quartz mon-zonite sample G95:040 have been handpicked and used for con-ventional U-Pb analysis. Titanite and monazite (one fraction each) were handpicked from granite sample G95:039 and ana-lysed. The analytical procedures used have been described by LARIONOV et al. (1995). All preparations and isotopic measure-ments were carried out at the Laboratory for Isotope Geology of the Swedish Museum of Natural History in Stockholm, using a Finnigan MAT 261 multi-collector mass spectrometer in sta-tic mode. The calculations were made with the programs of LUDWIG (1991a, 1991b), using the decay constants recommen-
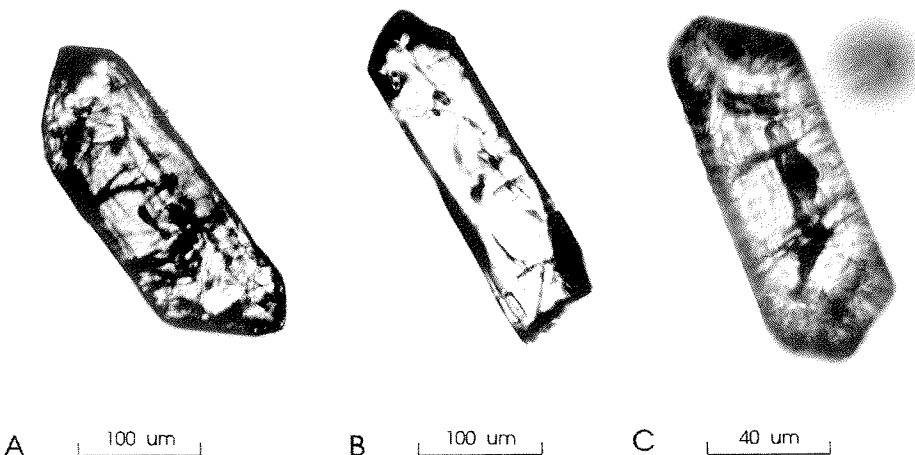

A ⌞ 100 um ⌟   B ⌞ 100 um ⌟   C ⌞ 40 um ⌟

Fig. 6: Photomicrographs of zircons from the Djupkilsodden quartz monzonite and granite.
A: turbid prismatic zircon from sample G95:038.
B: clear prismatic zircon from sample G95:038.
C: turbid prismatic zircon from sample G95:039.

Abb. 6: Mikroskopfotos von Zirkonen des Djup-kilsodden-Quarzmonzonits und -Granits.
A: trüber prismatischer Zirkon von Probe G95:038.
B: klarer prismatischer Zirkon von Probe G95:038.
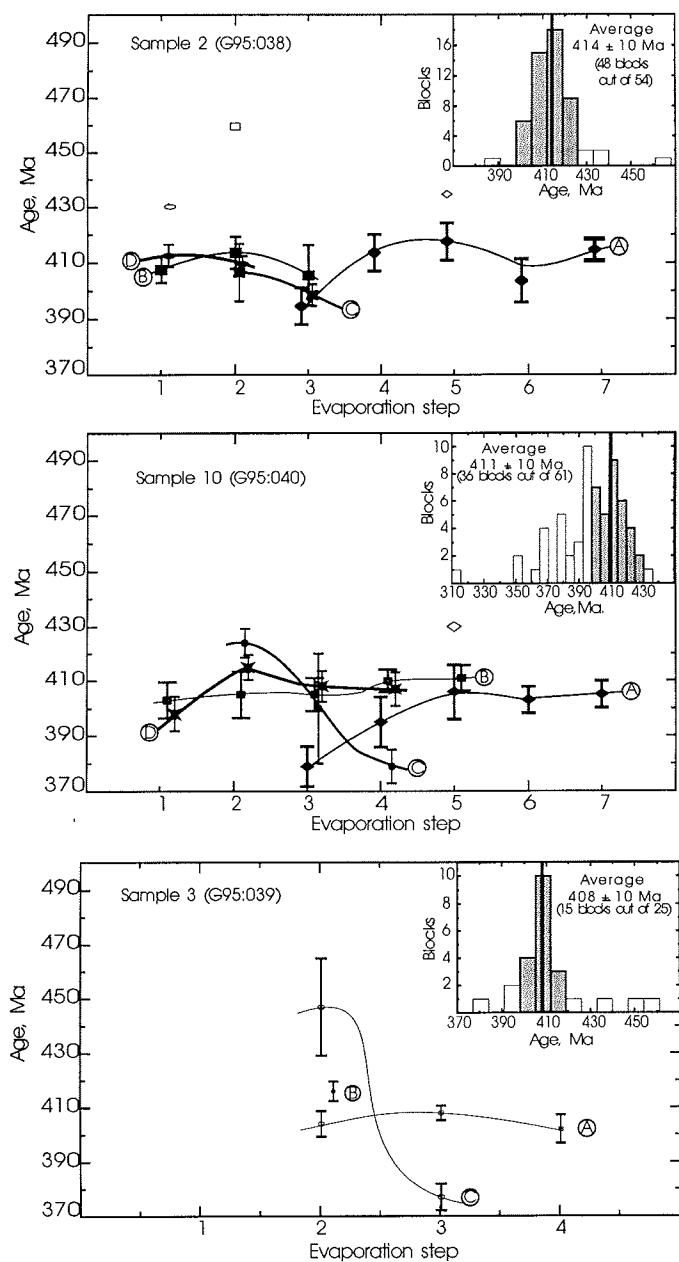**C:** trüber prismatischer Zirkon von Probe G95:039.

Fig. 7: Single zircon Pb evaporation results from the Djupkilsodden quartz monzonite and granite. A: sample G95:038. B: sample G95:040. C: sample G95:039. The main diagrams show the age results step by step for each grain, with outlying blocks shown as symbols without error bars. The inset histograms show all blocks, with those included in the average age calculation indicated by shading.

Abb. 7: Pb-Analysenergebnisse (KOBER-Methode) einzelner Zirkone des Djupkilsodden-Quarzmonzonits und -Granits. A: Probe G95:038. B: Probe G95:040. C: Probe G95:039. Die Hauptdiagramme zeigen die Altersergebnisse schrittweise für jeden Zirkon, wobei die abweichenden Blöcke durch Symbole ohne Toleranzbereich markiert sind. Die eingefügten Histogramme zeigen alle Blöcke, wobei die schattierten in die Berechnung des Durchschnittsalters einbezogen wurden.

ded by STEIGER & JÄGER (1977), and the corrections specified in the footnote to Tab. 4.

The results are listed in Tab. 4 and illustrated in Fig. 8. The zircons contain 500-700 ppm U and 35-50 ppm radiogenic Pb, while common Pb ranges between 0.42 and 1.15 ppm. They are

moderately discordant, and the $^{207}Pb/^{206}Pb$ ages for the individual fractions range between 414 and 429 Ma. If all seven points are combined, an ill-defined upper intercept age of 417 +104/-12 Ma is obtained, with lower intercept at -40 Ma and MSWD 5.5. Most of the scatter is due to the two coarsest fractions (points Zr3 and Zr7), which are plotting to the right of the regression line, probably due to inherited components in these large zircons. Excluding those two points gives a better defined upper intercept age of 417 +18/-7 Ma, with a lower intercept at 20 Ma and a MSWD of 0.32 (Fig. 8). An even better defined age, 416 ± 3 Ma, may be obtained by taking the average $^{207}Pb/^{206}Pb$ age of those five fractions; this may be justified considering that the lower intercept of the regression line is close to 0 Ma.

The titanite from granite sample G95:039 is unusually rich in U (545 ppm) and radiogenic Pb (35 ppm) for being titanite, but plots more discordantly than the zircon fractions and somewhat to the right of the zircon discordia (Fig. 8), suggesting the presence of some inheritance also in this mineral. However, the high degree of discordancy makes this uncertain, and little meaningful age information can be deduced from the titanite. The monazite is very rich in U (4660 ppm) and radiogenic Pb (2130 ppm). As normal for monazite, the thorogenic Pb component (^{208}Pb) dominates over the uranogenic one (^{206}Pb and ^{207}Pb). Unlike the titanite, the monazite plots concordantly at about 405 Ma ($^{207}Pb/^{235}U$ and $^{206}Pb/^{238}U$ ages; Fig. 8), about 10 Ma younger than the U-Pb zircon upper intercept age, and also slightly younger than concordant monazite from the nearby Rijpfjorden granite (412 Ma; JOHANSSON & LARIONOV 1996). This discrepancy may be attributed to a slightly lower intrusion age for the Djupkilsodden granite (sample G95:039) compared to the quartz monzonite (samples G95:038 and G95:040) as well as to the Rijpfjorden granite, or to the monazite recording cooling through its blocking temperature a few million years after the intrusion and crystallization of these rocks.

There is good agreement between the Pb-Pb single zircon and U-Pb multi-grain analyses, both methods indicating an age of c. 410-420 Ma for the composite Djupkilsodden quartz monzonite - granite pluton. The slight tendency for a higher age by the U-Pb multi-grain method may be explained by the presence of small amounts of older, inherited components in some of the grains. U-Pb ages on zircons from the neighbouring Rijpfjorden granite, on the other hand, scatter widely, probably due to inheritance (JOHANSSON & LARIONOV 1996, unpubl. data). From the above data, we conclude that the high-magnetic Djupkilsodden pluton has an intrusion age of c. 415 Ma, establishing the presence of late Silurian or early Devonian (TUCKER & MCKERROW 1995) magmatic activity in north-central Nordaustlandet. The more widely exposed Rijpfjorden granite is of about the same age, and may well be related to the same tectonomagmatic event.

No[1]	Size fraction (µm)	Weight (mg)	Concentrations, ppm			Measured ratios[2]			Radiogenic isotope ratios[3]			Err. corr.[4]	Calc. Ages (Ma)		
			U	Pb_{rad}	Pb_{com}	$\frac{^{206}Pb}{^{204}Pb}$	$\frac{^{206}Pb}{^{207}Pb}$	$\frac{^{206}Pb}{^{208}Pb}$	$^{207}Pb/^{235}U$ ± 28	$^{206}Pb/^{238}U$ ± 28	$^{207}Pb/^{206}Pb$ ± 28		$\frac{^{207}Pb}{^{235}U}$	$\frac{^{206}Pb}{^{238}U}$	$\frac{^{207}Pb}{^{206}Pb}$
Sample 2 (G95:038): Quartz monzonite															
Zr1	< 74	0.4280	667	44.3	0.50	4690	17.27	5.061	0.4715 10	0.06207 7	0.05510 9	0.590	392	388	416
Zr2	74-106	0.6190	690	44.7	0.51	4880	17.28	5.637	0.4660 10	0.06136 7	0.05508 10	0.562	388	384	415
Zr3	106-150	0.6957	691	44.2	0.42	5850	17.36	5.992	0.4657 10	0.06110 7	0.05528 9	0.627	388	382	424
Zr4	>150	0.2567	567	38.1	0.59	3330	16.96	5.327	0.4814 12	0.06332 7	0.05513 12	0.537	399	396	418
Sample 3 (G95:039): Granite															
Ti	all sizes	0.3574	545	35.3	2.38	805	13.68	3.252	0.4364 26	0.05689 17	0.05564 28	0.573	368	357	438
Mz	all sizes	0.2478	4661	2128	7.17	2620	16.56	0.1426	0.4908 16	0.06486 10	0.05488 15	0.549	405	405	408
Sample 10 (G95:040): Quartz monzonite															
Zr5	<74	0.1333	695	47.9	1.15	2130	16.36	4.516	0.4824 14	0.06349 8	0.05510 14	0.499	400	397	416
Zr6	74-106	0.2995	519	35.9	0.77	2460	16.54	4.496	0.4818 17	0.06349 8	0.05504 17	0.468	399	397	414
Zr7	>106	0.5438	656	44.0	1.14	2210	16.18	5.031	0.4809 13	0.06295 6	0.05540 13	0.462	399	394	429

Tab. 4: U-Pb data for zircons, titanite and monazite from the Djupkilsodden granitoids, north-central Nordaustlandet, Svalbard.
[1] Zr = Zircon, Ti = Titanite, Mz = Monazite; [2] Corrected for fractionation and blank, $^{206}Pb/^{204}Pb$ corrected for fractionation only. [3] All ratios corrected for fractionation (U according to analyses with $^{233-235}U$-tracer, Pb with 0.11 ± 0.04 % per AMU), blank (0.044-0.050 ng U and 0.015- 0.021 ng Pb with $^{206}Pb/^{204}Pb$ =18.7, $^{207}Pb/^{204}Pb$ =15.6, $^{208}Pb/^{204}Pb$ = 38.6) and common lead ($^{206}Pb/^{204}Pb$ =18.080, $^{207}Pb/^{204}Pb$ =15.595, $^{208}Pb/^{204}Pb$ = 37.894, STACEY & KRAMERS (1975) model value for 400 Ma). Errors reported as 2 standard deviations in the last decimals. [4] Error correlation $^{207}Pb/^{235}U$-$^{206}Pb/^{238}U$.

Tab. 4: U-Pb-Daten für Zirkon, Titanit und Monazit der Djupkilsodden-Granitoide, nördlicher Teil von Zentral-Nordaustlandet, Svalbard.
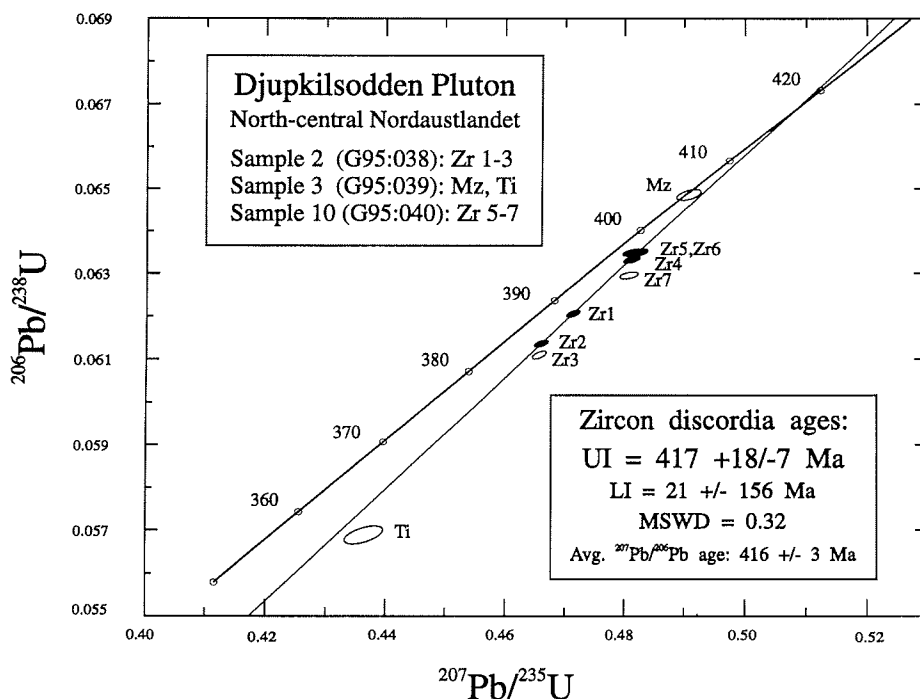

Fig. 8: Concordia diagram for zircons from the Djupkilsodden quartz monzonite (samples G95:038 and G95:040), and titanite and monazite from the Djupkilsodden granite (sample G95:039). Size of symbols reflects analytical uncertainty (28 errors), numbering refers to Table 4. Points Zr3 and Zr7, as well as the titanite and monazite points (unfilled symbols), have been excluded from the age calculations.

Abb. 8: Konkordia-Diagramm für Zirkone des Djupkilsodden-Quarzmonzonits (Proben G95:038 und G95:040), sowie Titanit und Monazit des Djupkilsodden-Granits (Probe G95:039). Die Symbolgröße ist ein Maß für die analytische Unsicherheit (28 Fehler), die Numerierung bezieht sich auf Tabelle 4. Die Punkte Zr3 und Zr7 sowie die Titanit- und Monazitpunkte (leere Symbole) sind nicht in die Altersberechnungen einbezogen worden.

5. DISCUSSION AND CONCLUSIONS

The unambiguous evidence presented here, that the strong magnetic anomaly of inner Duvefjorden is related, at least in part, to the highly magnetic Djupkilsodden quartz monzonite - granite pluton and that the latter is late Silurian or early Devonian in age is important for our understanding of Caledonian Svalbard. It also places constraints on interpretations of the offshore geology of the northwestern Barents Shelf and relationships between Barentsia (GEE & ZIEGLER 1996) and other early Palaeozoic terranes composing the Barents Sea basement. The re-

sults reported here identify a new major component of felsic plutonism that appears to be a part of a 300 km long linear belt of intrusions, reaching from the vicinity of Edgeøya to the northern edge of the Barents Shelf.

Late Caledonian, in general post-tectonic, felsic intrusions are conspicuous components of Svalbard's preDevonian basement. The isotopic age constraints are variable in quality, but all these intrusions appear to be Silurian or early Devonian, intruded into a consolidated crystalline crust after the main phase of Caledonian tectonism. Some are highly magnetic (e.g. the Hor-

nemantoppen batholith of northwestern Spitsbergen); others (e.g. the Newtontoppen batholith of southern Ny Friesland and the Rijpfjorden granite of Nordaustlandet) lack a clear magnetic signature.

Only the Newtontoppen batholith of southern Ny Friesland shows the same transition from quartz monzonite or quartz syenite to normal granite and the same S-type geochemistry (Fig. 5) as the Djupkilsodden intrusion. The Hornemantoppen batholith in northwestern Spitsbergen follows a more granodioritic trend (Figs. 5B, 5D) and is clearly I-type (Fig. 5F). Both are Caledonian in age (410-430 Ma, Rb-Sr whole rock method; HJELLE 1979, BALASOV et al. 1996, TEBENKOV et al. 1996). There is no aeromagnetic anomaly associated with the Newtontoppen batholith, while the Hornemantoppen batholith yields a strong positive aeromegnetic anomaly. The latter differs significantly from the Djupkilsodden Pluton, not only in geochemistry, but also has much higher magnetic susceptibility (up to 15 000 x 10^{-5} SI-units, A.M. Tebenkov, unpubl. data).

The Rijpfjorden granite, which outcrops circa 8 km west of the Djupkilsodden Pluton (Fig. 3, cf. map by FLOOD et al. 1969), and yields U-Pb monazite and Pb-Pb single zircon ages of 410-430 Ma (JOHANSSON & LARIONOV 1996, unpubl. data), is a normal granite (Figs. 5B, 5C, 5D). It differs petrochemically from the Djupkilsodden rocks on the K_2O-Na_2O diagram (Fig. 5F), where it is dominantly I-type. The difference may be connected with contamination of the relatively small bodies and dikes of the Djupkilsodden intrusion by surrounding biotite-rich migmatites and grey granites, although U-Pb and Pb-Pb zircon investigations (JOHANSSON & LARIONOV 1996, unpubl. data) suggest more extensive crustal contamination in the Rijpfjorden granite than in the Djupkilsodden quartz monzonite. Only the northwestern part of the Rijpfjorden granite shows up as a weak positive aeromagnetic anomaly (circa +100 nT; Fig. 2), whereas most of the outcrop area is aeromagnetically negative.

Offshore, to the east of Nordaustlandet, there occurs a variety of strong positive anomalies (F on Fig 2) that may be related to rock units of the Caledonian basement or to younger, Mesozoic intrusions. Major metagabbro bodies in the easternmost Nordaustlandet basement have low magnetic susceptibilities and it is therefore unlikely that these or similar intrusions provide the source for the offshore anomalies. Bottom samples (ELVERHØI et al. 1988) may provide some clues to the origin of the latter. Of particular importance for interpreting the eastern extension of the Nordaustlandet terrane will be the investigation of the age of the Kvitøya bedrock where existing descriptions of migmatites, granites, dolerites and gabbros (HJELLE 1978, HJELLE et al. 1978, OHTA 1978) suggest close affinity to Nordaustlandet.

The offshore belt of strong magnetic anomalies (G on Fig. 2), extending from near eastern Edgeøya northeastwards, via Kong Karls Land, to the offshore area south of Kvitøya, appears to be discordant to the N-S-trending central Nordaustlandet anomalies. The occurrence of late Jurassic to early Cretaceous basaltic volcanism on Kong Karls Land (cf. LAURITZEN & OHTA 1984) suggests that this NE-trending belt of anomalies is related to

Mesozoic rifting (cf. BAILEY & RASMUSSON 1997). The latter may well be controlled by older, Caledonian structures, marking the eastern boundary of Svalbard´s Eastern (Nordaustlandet) Terrane.

ACKNOWLEDGEMENTS

References

AMAROK A.S. (1994): Magnetic mapping of the Barents Sea (MMBS). Interpretation report prepared by Myklebust, R., Faleide, J.I., Gudlaugsson, S.T., Verba, M. & Usov, S.- AMAROK A.S., Oslo, 207 pp.

Balasov, Ju.A., Peucat, J.J., Tebenkov, A.M., Ohta, Y., Larionov, A.N. & Sirotkin, A.N. (1996): Additional Rb-Sr and single-grain zircon dating of Caledonian granitoid rocks from Albert I Land, northwest Spitsbergen. – Polar Research 15:153-165.

Batchelor, R.A. & Bowden, P. (1985): Petrogenetic interpretation of granitoid rock series using multicationic parameters. – Chemical Geology 48:43-55.

Bailey, J.C. & Rasmusson, M.H. (1997): Petrochemistry of Jurassic and Cretaceous tholeiites from Kong Karls Land, Svalbard, and their relation to Mesozoic magmatism in the Arctic. – Polar Research 16:37-62.

Carlsson, P., Johansson, Å. & Gee, D.G. (1995): Geochemistry of the Palaeoproterozoic Bangenhuk granitoids, Ny Friesland, Svalbard. – GFF 117:107-119.

Debon, F. & Le Fort, P. (1983): A chemical-mineralogical classification of common plutonic rocks and associations. – Transactions of the Royal Society of Edinburgh, Earth Sciences 73 (for 1982): 135-150.

Elverhøi, A., Antonsen, P., Flood, S.B., Solheim, A. & Vullstad, A.A. (1988): Physical environment western Barents Sea 1:1 500 000. Shallow bedrock geology. – Norsk Polarinstitutt Skrifter no. 179D: 32 pp.

Flood, B., Gee, D.G., Hjelle, A., Siggerud, T. & Winsnes, T.S. (1969): The geology of Nordaustlandet, northern and central parts. – Norsk Polarinstitutt Skrifter no. 146: 139 pp + 1 map 1:250 000.

Gee, D.G. (1986): Svalbard's Caledonian terranes reviewed. – Geologiska Föreningens i Stockholm Förhandlingar 108: 284-286.

Gee, D.G. & Hellman, F.J. (1996): Zircon Pb-evaporation ages from the Smutsbreen Formation, southern Ny Friesland: new evidence for Caledonian thrusting in Svalbard´s Eastern Terrane. – Zeitschrift Geol. Wiss. 24:429-439.

Gee, D.G. & Tebenkov, A.M. (1996): Two major unconformities beneath the Neoproterozoic Murchisonfjorden Supergroup in the Caledonides of central Nordaustlandet, Svalbard. – Polar Research 15:81-91.

Gee, D.G. & Ziegler, P.A. (1996): TIMPEBAR, Basement Control on Basin Evolution. – In GEE, D.G. & ZEYEN, H.J. (eds.), Lithospheric Dynamics: Origin and Evolution of Continents. – EUROPROBE 1996, Uppsala University, 101-109.

Gee, D.G., Johansson, Å., Ohta, Y., Tebenkov, A.M., Krasil'scikov, A.A., Balashov, Yu.A., Larionov, A.N., Gannibal, L.F. & Ryungenen, G.F. (1995): Grenvillian basement and a major unconformity within the Caledonides of Nordaustlandet, Svalbard. – Precambrian Research 70:215-234.

Hellman, F.J., Gee, D.G., Johansson, Å. & Witt-Nilsson, P. (1997): Single-zircon Pb evaporation geochronology constrains basement-cover relationships in the Lower Hecla Hoek Complex of northern Ny Friesland, Svalbard. – Chemical Geology 137:117-134.

Hjelle, A. (1978): An outline of the pre-Carboniferous geology of Nordaustlandet. – Polarforschung 48:62-77.

Hjelle, A. (1979): Aspects of the geology of northwest Spitsbergen. – Norsk Polarinstutt Skrifter no. 167:37-62.

Hjelle, A. & Lauritzen, Ø. (1982): Geological map of Svalbard 1:500 000. Sheet 3G, Spitsbergen northern part. – Norsk Polarinstitutt Skrifter no. 154C: 15 pp + 1 map 1:500 000.

Hjelle, A., Ohta, Y. & Winsnes, T.S. (1978): The geology of northeastern Svalbard. – Norsk Polarinstitutt Årbok 1977: 7-24.

Johansson, Å., Gee, D.G., Björklund, L. & Witt-Nilsson, P. (1995): Isotope studies of granitoids from th Bangenhuk Formation, Ny Friesland Caledonides, Svalbard. – Geological Magazine 132:303-320.

Johansson, Å. & Gee, D.G. (in press): The Eskolabreen granitoids of southern Ny Friesland, Svalbard Caledonides – geochemistry, age and origin. – GFF (submitted).

Johansson, Å. & Larionov, A.N. (1996): U-Pb ages from the Eastern Terrane of the Svalbard Caledonides – Evidence for Palaeoproterozoic, Grenvillian and Caledonian tectonism (extended abstract). – GFF 118 (Jubilee Issue): A38-A39.

Kober, B. (1986): Whole grain evaporation for 207Pb/206Pb age investigations on single zircons using a double filament thermal ion source. – Contributions to Mineralogy and Petrology 93:482-490.

Kulling, O. (1934): Scientific results of the Swedish-Norwegian Arctic Expedition in the summer of 1931, Part XI. The „Hecla Hoek Formation" round Hinlopenstredet. – Geografiska Annaler 16:161-254.

Larionov, A.N., Johansson, Å., Tebenkov, A.M. & Sirotkin, A.N. (1995): U-Pb zircon ages from the Eskolabreen Formation, southern Ny Friesland, Svalbard. – Norsk Geologisk Tidsskrift 75:247-257.

Larionov, A.N., Tebenkov, A.M. & Gee, D.G. (1998): Pb-Pb single-zircon ages of granitoid boulders from the Vendian tillite of Wahlenbergfjorden, Nordaustlandet, Svalbard. – Polar Research, 17:71-80.

Lauritzen, O. & Ohta, Y. (1984): Geological map of Svalbard 1:500 000. Sheet 4G, Nordaustlandet. – Norsk Polarinstitutt Skrifter no. 154D: 14 pp + 1 map 1:500 000.

Ludwig, K.R. (1991a): PBDAT – a computer program for processing Pb-U-Th isotope data, version 1.20 – U.S. Geol. Survey Open File Report 88-542, Denver.

Ludwig, K.R. (1991b): ISOPLOT – a plotting and regression program for radiogenic-isotope data, version 2.56. – U.S. Geol. Survey Open File Report 91-445, Denver.

Maniar, P.D. & Piccoli, P.M. (1989): Tectonic discrimination of granitoids. – Geol. Soc. Amer. Bull. 101:635-643.

Middlemost, E.A.K. (1985): Magmas and Magmatic Rocks: An Introduction to Igneous Petrology. – Longman, London, 266 pp.

Ohta, Y. (1978): Caledonian basic rocks of Storøya and Kvitøya, NE Svalbard. – Norsk Polarinstitutt Årbok 1977:25-42.

Ohta, Y. (1982): Relation between the Kapp Hansteen Formation and the Brennevinsfjorden Formation in Botniahalvøya, Nordaustlandet, Svalbard. – Norsk Polarinstitutt Skrifter no. 178:5-18.

Skilbrei, J.R. (1992): Preliminary interpretation of aeromagnetic data from Spitsbergen, Svalbard Archipelago (76-79 N): Implications for structure of the basement. – Marine Geology 106:53-68.

Skilbrei, J.R. (1993): Interpretation of geophysical data from the northwestern Barents Sea and Spitsbergen. – Geological Survey of Norway and University of Trondheim, Norwegian Institute of Technology.

Stacey, J.S. & Kramers, J.D. (1975): Approximation of terrestrial lead isotope evolution by a two-stage model. – Earth Planet. Sci. Letters 26:207-221.

Steiger, R.H. & Jäger, E. (1977): Convention on the use of decay constants in geo- and cosmochronology. – Earth Planet. Sci. Letters 36:359-362.

Tebenkov, A.M. (1996): Analiz vozmoznyh istochnikov magnitnyh anomalij na arhipelago Shpitsbergen i prilegajushem shelfe (Analyses of possible sources of magnetic anomalies on the Spitsbergen archipelago and surrounding shelf, in Russian). – In: G.P. AVETISOV (ed.): Geological-Geophysical Characteristics of the Lithosphere of the Arctic Regions. – VNII Oceangeology, St. Petersburg, 38-44.

Tebenkov, A.M., Ohta, Y., Balasov, Ju.A. & Sirotkin, A.N. (1996): Newtontoppen granitoid rocks, their geology, chemistry and Rb/Sr age. – Polar Research 15:67-80.

Tucker, R.D. & McKerrow (1995): Early Paleozoic chronology: a review in light of new U-Pb zircon ages from Newfoundland and Britain. – Canadian J. Earth Sci. 32:368-379.

Witt-Nilsson, P., Gee, D.G., & Hellman, F.J. (1998): Tectonostratigraphy of the Caledonian Atomfjella Antiform of northern Ny Friesland, Svalbard. – Norsk Geologisk Tidsskrift 78:67-80.

Appendix 1. Single-zircon Pb evaporation data from the Djupkilsodden granitoids, north-central Nordaustlandet, Svalbard.

Plating Step and Block	Plating T °C	Plating min.	Measured 206Pb/204Pb	Measured 207Pb/206Pb ±2s%	Calculated Age, Ma
I	1380	6	-	-	-
II	1410	5	-	-	-
III 1	1420	7	28594	0.0557204 1.04	421
2			100000	0.0556422 0.93	433
3			37476	0.0551592 2.02	403
IV 1	1430	5	100000	0.0554655 1.22	426
2			45570	0.0554322 1.22	417
3			100000	0.0553981 2.00	423
4			20000	0.0558210 1.44	416
V 1	1440	5	45906	0.0554957 1.52	420
2			54823	0.0558636 1.34	437
3			15395	0.0552820 1.28	385
VI 1	1450	6	21916	0.0554281 1.26	403
2			25193	0.0553837 2.04	405
3			20000	0.0554945 2.36	403
4			20000	0.0557284 1.53	413
VII 1	1470	6	61037	0.0552377 0.61	413
2			39323	0.0555553 0.77	420
3			34636	0.0553752 0.67	411
4			100000	0.0552459 0.66	417
5			100000	0.0554538 1.16	425
6			100000	0.0552394 1.02	416
7			54853	0.0551876 0.80	409
8			59479	0.0551320 0.68	408
9			64861	0.0554365 0.94	421

G95:038 Grain A: Euhedral, brownish, semi-transparent, fractured grain with black inclusion, somewhat flat. Facets (110)+(111).

Plating Step and Block	Plating T °C	Plating min.	Measured 206Pb/204Pb	Measured 207Pb/206Pb ±2s%	Calculated Age, Ma
I 1	1400	8	22622	0.0556180 1.04	412
2			13669	0.0559723 0.96	409
3			16702	0.0558828 1.38	413
4			12928	0.0557783 0.94	398
II 1	1410	12.5	19330	0.0556851 0.76	410
2			27373	0.0560769 1.52	462
3			19673	0.0557853 0.33	414
4			15023	0.0556733 1.72	400
III 1	1500	5	11168	0.0561924 2.63	408

G95:038 Grain B: Euhedral, pinkish, almost transparent, fractured grain with black inclusion. Facets (110)+(111).

Plating Step and Block	Plating T °C	Plating min.	Measured ^{206}Pb/^{204}Pb	Measured ^{207}Pb/^{206}Pb ±2s%	Calculated Age, Ma
I	1420	9	-	-	-
II 1	1460	10	30000	0.0554087 2.08	409
2			14659	0.0560113 2.14	413
3			25525	0.0554665 2.78	408
III 1	1500	5	23027	0.0553579 0.96	401

G95:038 Grain C: Subhedral, pinkish, almost colourless transparent grain, with black inclusion. Facets (110)+(111)+(121).

Plating Step and Block	Plating T °C	Plating min.	Measured ^{206}Pb/^{204}Pb	Measured ^{207}Pb/^{206}Pb ±2s%	Calculated Age, Ma
I 1	1420	6	10597	0.0566883 0.23	425
2			8745	0.0567370 0.70	415
3			17742	0.0563012 0.83	432
4			16768	0.0563910 0.98	434
5			10647	0.0563938 0.78	414
6			10321	0.0564671 0.55	415
7			9065	0.0566344 0.63	414
8			9929	0.0566761 0.81	421
9			9348	0.0566260 0.96	415
II 1	1450	5	23148	0.0555284 0.46	408
2			25218	0.0554283 0.56	407
3			26476	0.0556118 0.58	415
4			34301	0.0554896 0.42	415
5			22069	0.0555898 0.24	410
6			25806	0.0555440 0.45	412
7			23516	0.0557866 1.15	419
8			20639	0.0556317 0.58	410
9			18043	0.0556518 0.48	406

G95:038 Grain D: Euhedral, brownish, almost transparent, fractured grain. Facets (110)+(111). Some probably corroded spots noted at prism facets.

Plating Step and Block	Plating T °C	Plating min.	Measured ^{206}Pb/^{204}Pb	Measured ^{207}Pb/^{206}Pb ±2s%	Calculated Age, Ma
I	1410	4	-	-	-
II	1420	6	-	-	-
III 1	1420	6	18197	0.0553279 2.60	393
2			8450	0.0556215 1.26	367
3			7179	0.0555069 1.80	349
IV 1	>1420	8	39542	0.0552998 1.64	410
2			11246	0.0551571 1.54	366
3			8285	0.0559551 2.44	379
4			7844	0.0564583 2.04	396
5			7075	0.0558223 1.58	361
6			7553	0.0558251 1.60	367
7			4585	0.0558430 1.86	314
V 1	1440	7	26488	0.0548295 0.74	383
2			44610	0.0558657 2.22	434
3			26119	0.0547832 2.58	381
4			32796	0.0558032 1.82	427
5			18632	0.0552851 1.30	392
6			6053	0.0558955 1.42	350
VI 1	1450	5	14561	0.0551120 1.28	376
2			20991	0.0551967 0.92	392
3			26599	0.0553205 1.30	403
VII 1	1500	5	31136	0.0552147 1.20	402
2			22493	0.0552163 1.08	395
3			28302	0.0555888 0.89	416

G95:040 Grain A: Euhedral, pink, transparent grain, with black inclusion. Facets (110)+(111).

Plating Step and Block	Plating T °C	Plating min.	Measured ^{206}Pb/^{204}Pb	Measured ^{207}Pb/^{206}Pb ±2s%	Calculated Age, Ma
I	1420	6	-	-	-
II 1	1440	5	27709	0.0557980 1.23	424
III 1	1450	6	3601	0.0584246 2.56	387
2			5000	0.0578904 1.58	411
IV 1	>1500	10	5541	0.0568118 1.62	379

G95:040 Grain C: Euhedral, pink, transparent, long-prismatic grain. Facets (110)+(111)+(331).

Plating Step and Block	Plating T °C	Plating min.	Measured ^{206}Pb/^{204}Pb	Measured ^{207}Pb/^{206}Pb ±2s%	Calculated Age, Ma
I 1	1400	5	3681	0.0587379 1.62	403
II 1	1430	7	4541	0.0583511 1.14	418
2			3723	0.0587273 2.62	405
III 1	1450	7	5077	0.0580778 1.16	421
2			4537	0.0580247 0.88	405
3			3948	0.0584075 0.80	401
4			3999	0.0582788 0.89	397
5			4256	0.0584448 0.68	413
6			2987	0.0588201 2.30	368
IV 1	1460	7	32113	0.0553585 0.78	409
2			22413	0.0555616 1.72	409
3			25357	0.0553878 0.40	405
4			29943	0.0555464 0.54	415
V 1	1520	4	15734	0.0554824 0.40	394
2			42566	0.0554420 1.50	417

G95:040 Grain B: Subhedral, pink-yellowish, transparent grain, with chain of bubble-shaped inclusion in center. Facets (110)+(111)+(331).

Plating Step and Block	Plating T °C	Plating min.	Measured ^{206}Pb/^{204}Pb	Measured ^{207}Pb/^{206}Pb ±2s%	Calculated Age, Ma
I 1	1400	5	23818	0.0548750 0.58	382
2			20395	0.0552822 0.66	395
3			14691	0.0556185 1.64	397
4			30311	0.0552708 0.76	404
5			15591	0.0556510 1.72	401
II 1	>1400	5	82603	0.0553346 1.24	419
2			79341	0.0552676 0.84	416
3			76930	0.0553599 1.00	420
4			36417	0.0553439 1.36	410
5			85844	0.0549825 0.64	405
III 1	1420	5	11879	0.0558851 1.50	399
2			16081	0.0560957 1.46	420
3			16715	0.0557961 1.40	410
4			12332	0.0558030 0.62	397
5			16607	0.0558156 1.63	410
IV 1	1430	5	14174	0.0557571 1.14	402
2			14279	0.0564215 1.02	429
3			12362	0.0557394 1.40	395
4			13588	0.0560904 0.78	413
5			10711	0.0559150 1.72	394

G95:040 Grain D: Subhedral, pink-yellowish, transparent, twinned grain, with black inclusion in centre. Facets (110)+(111)+(331).

Plating Step and Block	Plating T °C	Plating min.	Measured ^{206}Pb/^{204}Pb	Measured ^{207}Pb/^{206}Pb ±2s%	Calculated Age, Ma
I 1	1350	10	430	0.0752122 3.44	100
II 1	>1370	7	3021	0.0596757 0.43	406
2			2920	0.0598675 0.76	407
3			2796	0.0599727 0.66	403
4			2672	0.0599856 0.64	393
5			2542	0.0603289 0.46	396
6			2653	0.0603862 0.46	408
7			2667	0.0604180 0.41	410
8			2588	0.0604536 0.33	405
9			2449	0.0606385 0.96	399
III 1	1420	7	5199	0.0577628 0.56	411
2			4922	0.0577854 0.84	405
3			4899	0.0578527 0.87	407
4			4927	0.0578611 0.52	409
5			4851	0.05576535 0.39	398
6			5300	0.0578700 0.50	417
IV 1	1430	5	3455	0.0592284 1.02	413
2			2919	0.0597502 0.90	402

G95:039 Grain A: Half of subhedral, brown, tranlucent grain, with somewhat corroded surface and a few inclusions. Facets (100)+(111).

Plating Step and Block	Plating T °C	Plating min.	Measured $^{206}Pb/^{204}Pb$	Measured $^{207}Pb/^{206}Pb$ ±2s%		Calculated Age, Ma
I	1250	5	-	-		-
II 1	>1270	7	2232	0.0615370	0.45	413
2			2141	0.0619671	0.58	419

G95:039 Grain B: Euhedral, pink, transparent in central part, but with turbid terminations, with a few black inclusions. Facets (100)+(111).

Plating Step and Block	Plating T °C	Plating min.	Measured $^{206}Pb/^{204}Pb$	Measured $^{207}Pb/^{206}Pb$ ±2s%		Calculated Age, Ma
I	1400	5	-	-		-
II 1	>1430	9.5	1624	0.0646230	2.18	439
2			1581	0.0640425	2.01	405
3			1735	0.0642841	2.00	448
4			1821	0.0640483	0.98	454
III 1	1420	7	3890	0.0578979	1.29	377

G95:039 Grain C: Euhedral, yellow-brownish, semi-transparent grain, surface a bit corroded. Facets (100)+(111).